DIFFRACTION BY A THICK IMPEDANCE EDGE AND AN IMPEDANCE STEP PROTRUSION

Final Report

by

John L. Volakis

and

Mark Ricoy

Radiation Laboratory
Department of Electrical Engineering and Computer Science
The University of Michigan
Ann Arbor, Michigan 48109

for

Rockwell International
North American Aircraft
P.O. Box 92098
Los Angeles, CA 90009

388967-1-F = RL-2555

September 1985

TABLE OF CONTENTS

LIST OF ILLUSTRATIONS

I. Introduction

An analytical study was performed for calculating the scattered field by a step protrusion shown in Fig. 1. Measured data were also collected and were found to be in good agreement with the analytical data.

Two independent methods were used to obtain analytical expressions: the angular spectrum method [1] and the geometrical theory of diffraction (GTD). The first becomes cumbersome for large $\ell(\ell > \lambda/4)$ and is thus suitable for protrusions of small thickness. In contrast, the GTD which is a high frequency method, becomes accurate and efficient for the analysis of thick ($\ell > \lambda/4$) protrusions. The accuracy of each technique in their respective regions of applicability was clearly demonstrated by the obtained measured data.

2. Analysis via the Angular Spectrum Method

Before proceeding with the application of this method, the protrusion geometry in Fig. 1 was broken down to a series of sub-geometries. First the diffraction by a pair of half planes (see Fig. 2) was obtained by imposing the appropriate impedance boundary conditions on the outer faces of the half planes. The details of this analysis are described in [2]. It was found that the diffracted field is given by

$$E_z^{sa} = D_S^I(\phi,\phi_0;n_1)\Delta(\phi,\phi_0;\ell)\frac{e^{-jkr}}{\sqrt{r}} \qquad (1)$$

for the E_z (plane wave) incidence. In the above $D_S^I(\phi,\phi_0)$ is the soft diffraction coefficient for the impedance half plane and is given by

$$D_S^I(\phi,\phi_0;\eta_1) = \frac{e^{-j\pi/4}}{\sqrt{2\pi k}} \frac{1 - 2\eta_1 \cos\phi/2 \cos\phi_0/2}{\cos\phi + \cos\phi_0} U_3(\cos\phi;\eta_1)U_3(\cos\phi_0;\eta_1) \ . \tag{2}$$

$\Delta(\phi,\phi_0;\ell)$ is defined by

$$\Delta(\phi,\phi_0;\ell) = e^{-jk\ell \sin\phi} \frac{L_1(\cos\phi_0)}{U_1(\cos\phi)} \cos(k\ell \sin\phi) + j \frac{L_2(\cos\phi_0)}{U_2(\cos\phi)} \sin(k\ell \sin\phi) \ . \tag{3}$$

In the case of H_z-incidence we obtain via duality that

$$H_z^{sa} = D_h^I(\phi,\phi_0;\eta_1)\Delta(\phi,\phi_0;\ell) \frac{e^{-jkr}}{\sqrt{r}} \ , \tag{4}$$

where

$$D_h(\phi,\phi_0;\eta_1) = D_s(\phi,\phi_0;1/\eta_1) \ . \tag{5}$$

The split functions $U_i(\cos\phi)$ and $L_i(\cos\phi)$ are defined in Appendices I and II of [2] and are in non-integral form. They may, however, appear cumbersome in form but do not present any computational difficulty. It is further noted that (1) and (4) will reduce to the known result for the perfectly conducting $\eta_1 \to 0$.

The next geometry in progression is created by adding a stub with an impedance surface between the half planes as shown in Fig. 3. Subsequently, by letting $d \to 0$ one can obtain the diffraction by a thick impedance edge. In turn, image theory can be invoked for the analysis of the original step protrusion shown in Fig. 1. Specifically, we have that

$$E_z^{sP}(\phi,\phi_o) = E_z^{sHP}(\phi,\phi_o) - E_z^{sHP}(\phi,2\pi - \phi_o)e^{-2jk\ell \sin \phi_o} \qquad (6)$$

and

$$H_z^{sP}(\phi,\phi_o) = H_z^{sHP}(\phi,\phi_o) - H_z^{sHP}(\phi,2\pi - \phi_o)e^{-2jk\ell \sin \phi_o} \quad . \qquad (7)$$

In the above E_z^{sP} and H_z^{sP} denote the scattered fields in the presence of the ground plane while E_z^{sHP} and H_z^{sHP} correspond to the scattered fields by the impedance half plane of thickness twice that of the step.

When the ground plane is replaced by an impedance plane, (6) and (7) are not valid and must be modified as discussed in [2].

The analysis of the geometry in Fig. 3 involves the coupling of the incident field to waveguide modes, the reflection of these modes from the stub, the subsequent re-radiation of the modes as well as their multiple interactions between the waveguide opening and the stub. Since the final geometry of interest is the thick impedance edge in Fig. 2, we may assume in this analysis that the inner walls of the parallel plate waveguide are perfectly conducting without loss of generality. Further, by restricting $\ell < \lambda/2$, all modes other than the TEM mode are attenuating and can therefore be neglected for a first order analysis. The TEM mode exists only in the case of H_z-incidence and thus the results in (1) for the E_z-incidence is a good approximation for the thick impedance edge when $\ell < \lambda/4$.

Inclusion of the TEM mode (and all of its multiple interactions) for the H_z incidence results to the following expression for the diffracted field from a thick impedance edge:

$$H_z^s = H_z^{sa} + \frac{e^{-j\pi/4}}{\sqrt{2\pi k}} \frac{e^{-jkr}}{\sqrt{r}} \frac{C_o(\phi_o)\Gamma_o L_o(\phi)}{1 - \Gamma_o R_o} \qquad (8)$$

where

$$C_0(\phi_0) = \frac{L_{2+}(\cos \phi_0)}{U_{2+}(1)} \tag{9}$$

$$L_0(\phi) = \frac{2j\, e^{-jk\ell \sin \phi}}{\cos \phi/2} \frac{L_2(1)}{U_2(\cos \phi)} \sin(k\ell \sin \phi) \tag{10}$$

$$R_0 = - \frac{L_{2+}(1)}{U_{2+}(1)} \tag{11}$$

$$\Gamma_0 = \frac{\eta_1 - 1}{\eta_1 + 1} \tag{12}$$

$$L_2(\cos \phi) = 2\sqrt{k\ell} \sin \phi/2\, L_{2+}(\cos \phi) \tag{13a}$$

and

$$U_2(\cos \phi) = 2\sqrt{k\ell} \cos \phi/2\, U_{2+}(\cos \phi) \, . \tag{13b}$$

According to Fig. 4, C_0 is referred to as the coupling coefficient, L_0 as the launching coefficient, R_0 as the reflection coefficient and Γ_0 is the plane wave reflection coefficient from the impedance stub.

It is noted that the inclusion of the TEM mode was done as if the two parallel half planes were perfectly conducting [3]. However, such an approximation is not expected to compromise the accuracy of the results [4] since the coupling effect is dominant when ϕ is near 180 degrees where our assumption is valid.

The accuracy of the above analysis can be improved (especially for the E_z-incidence) by the inclusion of additional modes. Expressions for the coupling, launching and reflection coefficient have already been obtained via the angular spectrum method and we are currently in the process of including them in the computer program.

3. Analysis via the Geometrical Theory of Diffraction

As mentioned earlier, this analysis assumes that 2ℓ is large ($> \lambda/2$). Using GTD one can obtain the scattering from a thick edge (see Fig. 5) in a direct manner. Assuming that the surface coating is lossy, one needs to only consider the first order mechanisms illustrated in Fig. 5. The individual contribution of each of these mechanisms requires the use of the diffraction coefficient for a right angled impedance wedge which is given in [5]. The diffracted field by a step protrusion is obtained via image theory according to Eqs. (6) and (7).

However, in case of a perfectly conducting thick edge or step ($\eta_1 = 0$) one should also include the contribution of the higher order mechanisms illustrated in Fig. 6. These need only be included in the H_z-incidence case since they give zero field in case of E_z-incidence. Analytical expressions for the higher order fields were obtained in a closed form via the self-consistent GTD approach.

4. Comparison of Calculations with Measured Data

An extensive number of backscatter measurements were collected in order to verify the analysis discussed earlier and in [2]. The major problem in collecting measured data for theory verification purposes is the construction of appropriate test models. In this case our test model must isolate the backscattering by a single thick edge. One such test model is shown in Fig. 7. Provided all measurements are performed in the xy-plane (see Figs. 1 and 5), the only backscatter mechanisms will be from the front edge located at $x = 0$. Any scattering by the rear tip and the side edges will be negligible. In order to further reduce the scattering due to interactions between the side edges,

magnetic absorber strips were initially placed around the side edges when performing measurements with the perfectly conducting thick edge. This is shown in Fig. 7. However, it was found that such a precaution was not necessary.

An appropriate test model for a step protrusion on the gound plane is illustrated in Fig. 8. Based on the ground plane length in front of the step, it is concluded that the ground plane effect will be present to within five degrees of the edge-on incidence (ϕ = 180 degrees).

The analysis discussed earlier was restricted to two-dimensional geometries (see Figs. 1 through 6). However, since the test models are of finite extent along the z-direction, a relationship is required between the measured and calculated results. Using the equivalent current concept it is found that the radar cross section of a finite length edge is given by

$$\sigma_{3\text{-}D} = \frac{4\pi}{k} Z_d^2 \sigma_{2\text{-}D} \tag{14}$$

where Z_d is the length of the edge,

$$\sigma_{2\text{-}D} = \lim_{r \to \infty} 2\pi r \frac{|E_z^s|^2}{|H_z^s|^2} \tag{15}$$

is the echo width of the edge and E_z^s with H_z^s denote the total scattered field. For the models in Figs. 7 and 8, Z_d = 1.5 ft.

Measurements were performed at 9 GHz on two thick edge models corresponding to thicknesses 2ℓ = 0.614 inch and 2ℓ = 1.0 inch. Both of these were measured without coating, however, only the first was tested with a 0.03 inch material coating. This coating was characterized with a relative permittivity of ε_r = 20-j1 and μ_r = 1.4-j1.5 corresponding to η = 0.689 + j.812. Measurements were also performed on the step protrusion model shown in Fig. 8 with ℓ = 0.307, i.e., half the thickness of the first thick edge model. The material coating was placed on the step protrusion model as illustrated in Fig. 1.

Figure 9 presents a comparison of the measured and calculated backscatter patterns from a perfectly conducting edge with 2ℓ = 0.614 inch. As seen for the H_z-incidence the angular spectrum method is in excellent agreement with the measured data. A good agreement is also observed for the E_z-incidence. However, as indicated earlier, in case of the E_z-incidence the angular spectrum method needs to be improved by the inclusion of additional modes. It is further noted that the ripple in the measured patterns is due to the interactions between the front edge and the rear tip. We also observe in Fig. 9 that the GTD patterns are in remarkable agreement with the measured patterns for either the E_z or H_z cases. This clearly indicates that the simple GTD analysis is applicable to thicker edges ($2\ell > \lambda/2$). Such a statement is verified in the edge on echowidth plot of Fig. 10. It is observed that the ideal changeover point from the angular spectrum method to the GTD is at $2\ell \approx \lambda/2$. As a result, in the patterns of Fig. 11 which correspond to a perfectly conducting edge with 2ℓ = 1.0 inch, the GTD patterns nearly overlay the measured patterns corresponding to the model in Fig. 7.

When the aforementioned coating is placed over the thick edge with 2ℓ = 0.614 inch, the results for the H_z and E_z incidences are shown in Figs. 12(a) and 12(b), respectively. The agreement between measured and calculated patterns is not as good as that observed for the perfectly conducting case. This is probably due to the test model accuracy in representing the computer model.

The patterns given in Figs. 13 and 14 constituted the primary objective of this research. Clearly a good agreement is observed between measured and calculated data for both the perfectly (Fig. 13, H_z and E_z incidences) and imperfectly (Fig. 14, H_z and E_z incidences) step protrusion on a ground plane. A comparison of the H_z and E_z patterns indicates the high cross section associated with the H_z case when at edge-on (ϕ = 180 degrees). The cross sections for the E_z case vanishes at edge-on incidence.

5. Family and Design Curves

The presentation of the measured data in the previous section served as a verification of the accuracy of our analytical models. Now that the degree of this accuracy has been established we may proceed to obtain a series of patterns for edges and step protrusions as a function of the thickness 2ℓ. The following collection of patterns refer to the geometries in Figs. 1 and 5.

Figures 15 through 18 each contain ten backscatter patterns corresponding to a specific value of $2\ell/\lambda$. Among those patterns 2ℓ ranges from 0.01λ to λ. Note that the case of $2\ell = 0.468\lambda$ corresponds to the thickness of the test model. The patterns corresponding to $2\ell < 0.5\lambda$ were computed via the angular spectrum method whereas the

patterns with $2\ell > 0.5\lambda$ were computed via the GTD (see Fig. 10). Family curves of the echowidth for both polarizations are included. Figures 15 and 17 refer to a perfectly conducting and imperfect thick edge geometry shown in Fig. 5. In addition, Figs. 16 and 18 refer to a perfectly conducting and imperfect step protrusion on a ground plane as shown in Fig. 1.

References

1. P. C. Clemmow, "A method for the exact solution of a class of two-dimensional diffraction problems," Proc. Royal Soc. A (205), pp. 286-308, 1951.

2. J. L. Volakis, "Diffraction by a pair of impedance half-planes and an impedance half-plane on a ground plane", The University of Michigan, Radiation Laboratory Report No. 388967-1-T, May 1985.

3. S-W Lee and R. Mittra, "Diffraction by a thick conducting half plane and a dielectric-loaded waveguide," IEEE Trans. Antennas and Propagat., AP-16, No. 4, pp. 454-461, July 1967.

4. T.B.A. Senior and J. L. Volakis, "Scattering by an imperfect right angled wedge," submitted to IEEE Trans. on Antennas and Propagat.

5. G. D. Maliuzhinets, "Excitation, reflection and emission of surface waves from a wedge with given face impedances," Sov. Phys. Dokl., pp. 752-755, 1958.

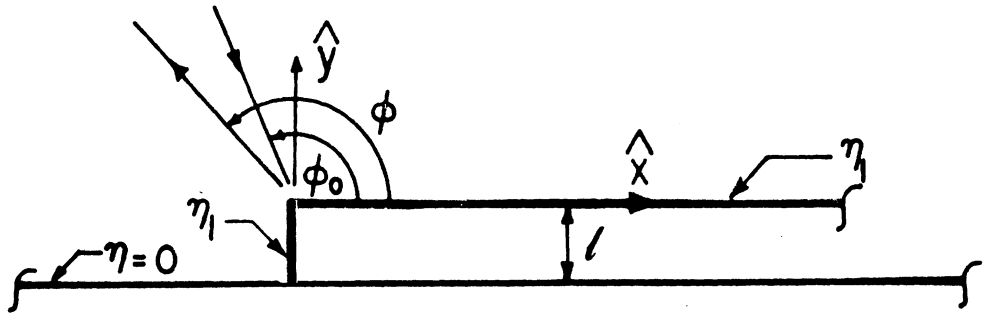

Fig. 1: Geometry of a step protrusion with a surface impedance η_1 as shown.

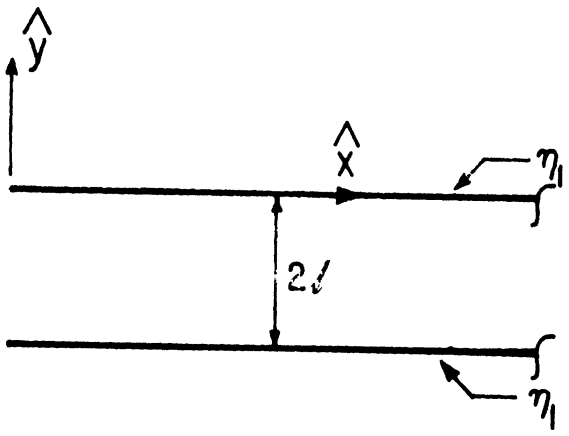

Fig. 2: Geometry of a pair of parallel half-planes with a surface impedance η_1 on their outer surfaces.

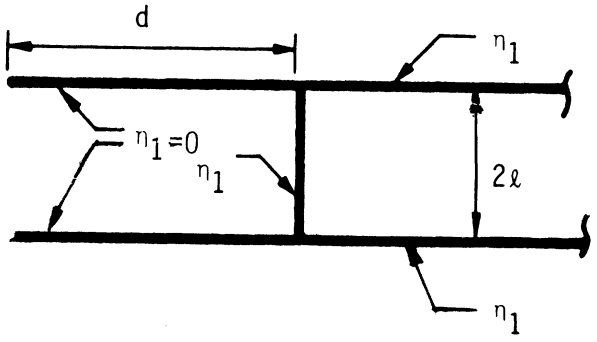

Fig. 3: Two half-planes with an impedance stub inserted. d = 0 constitutes a thick half-plane.

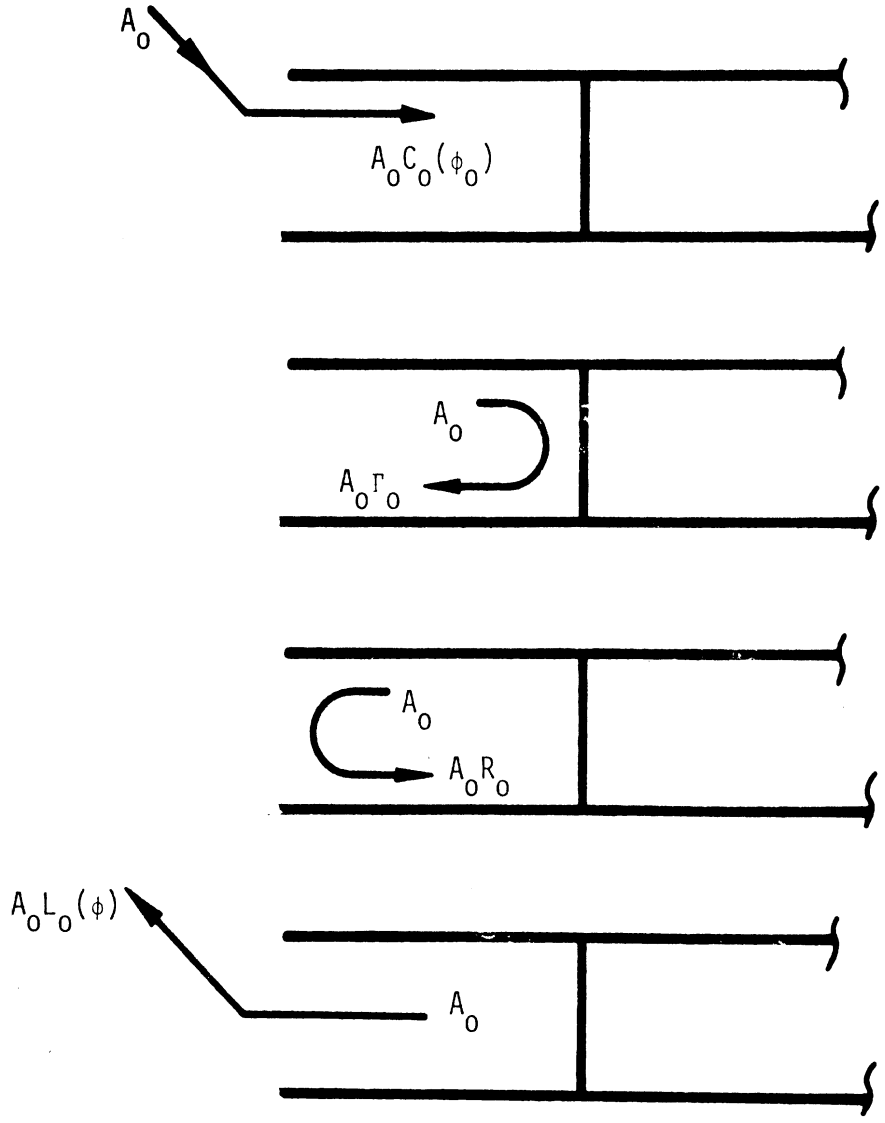

Fig. 4: Illustration of the coupling, reflection and launching coefficients.

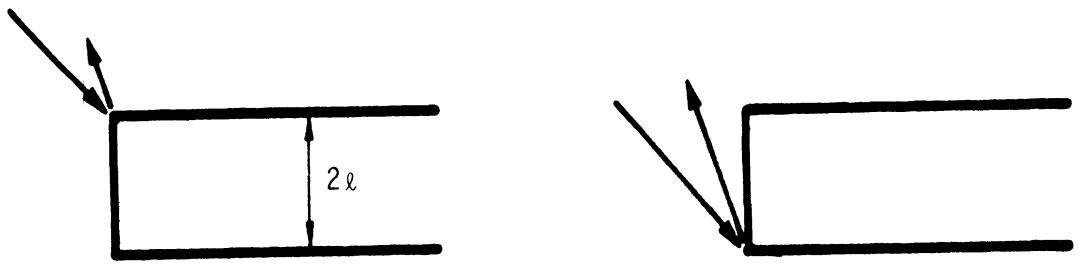

Fig. 5: First order diffraction mechanisms from a thick edge.

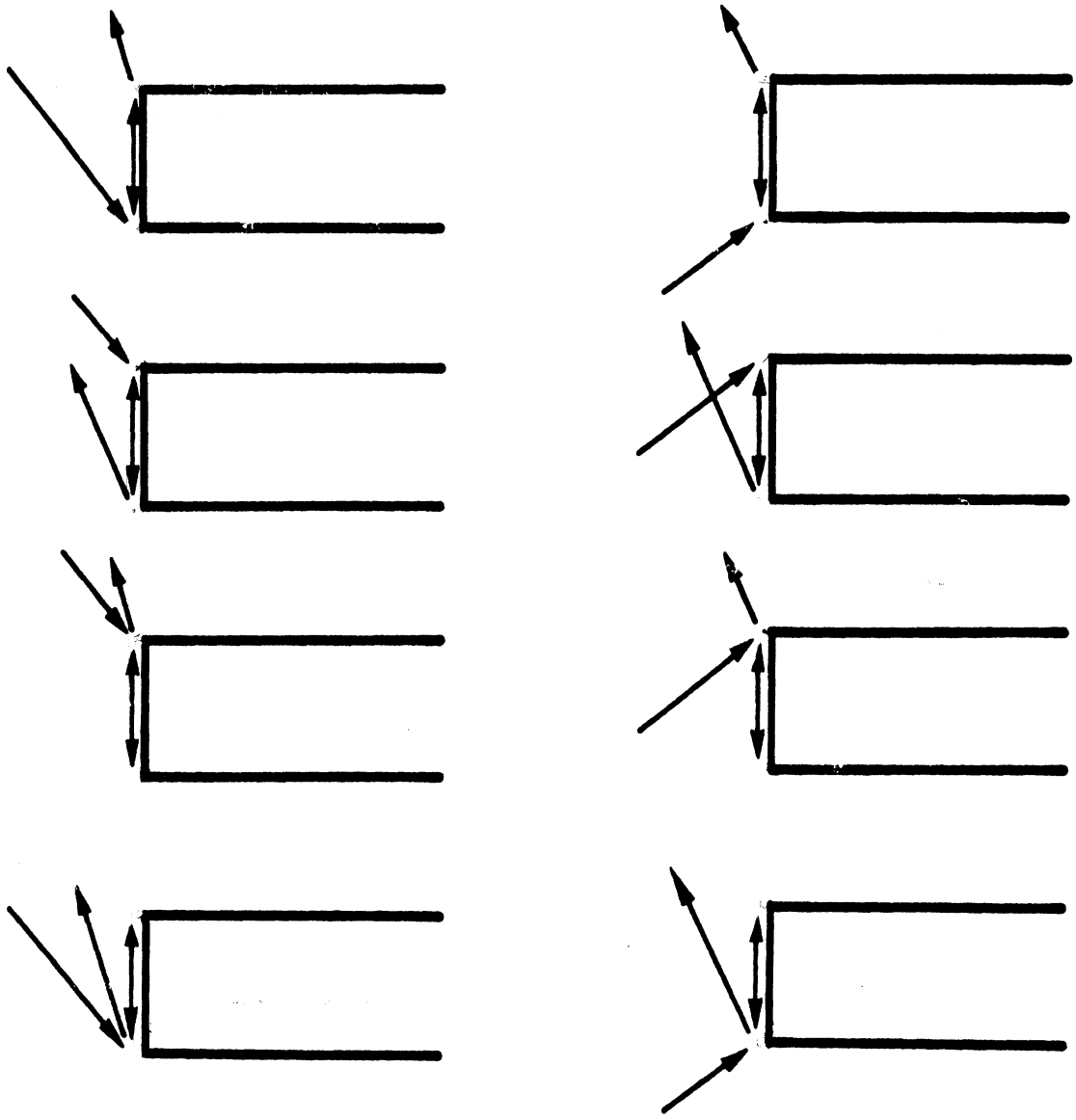

Fig. 6: Higher order diffraction mechanisms from a thick edge. (a) Direct wave. (b) Image wave.

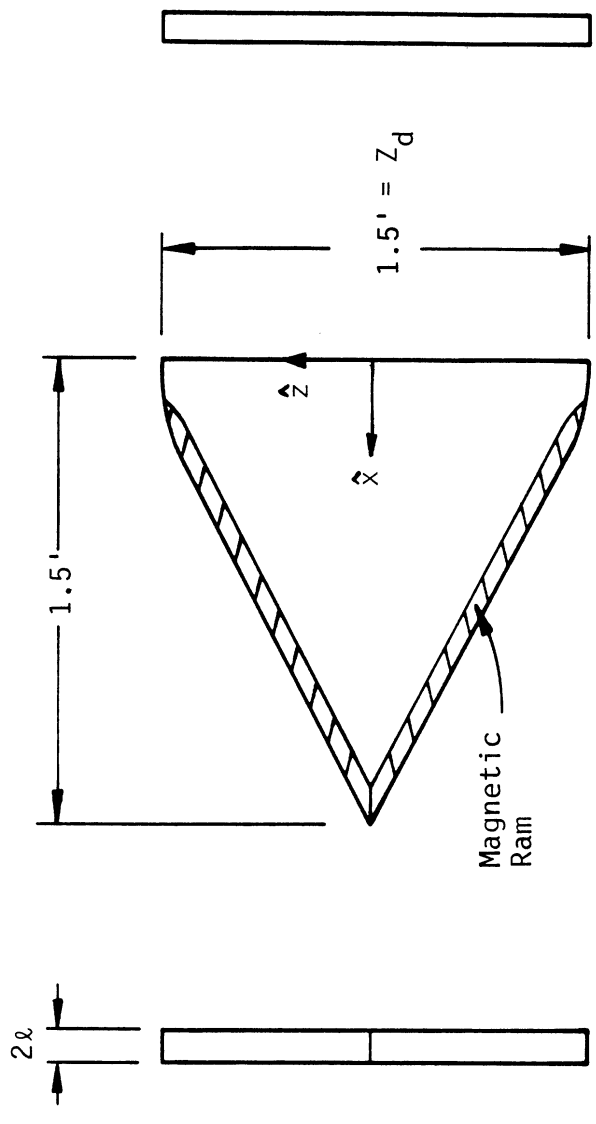

Fig. 7: Measurement Model of a Thick Edge

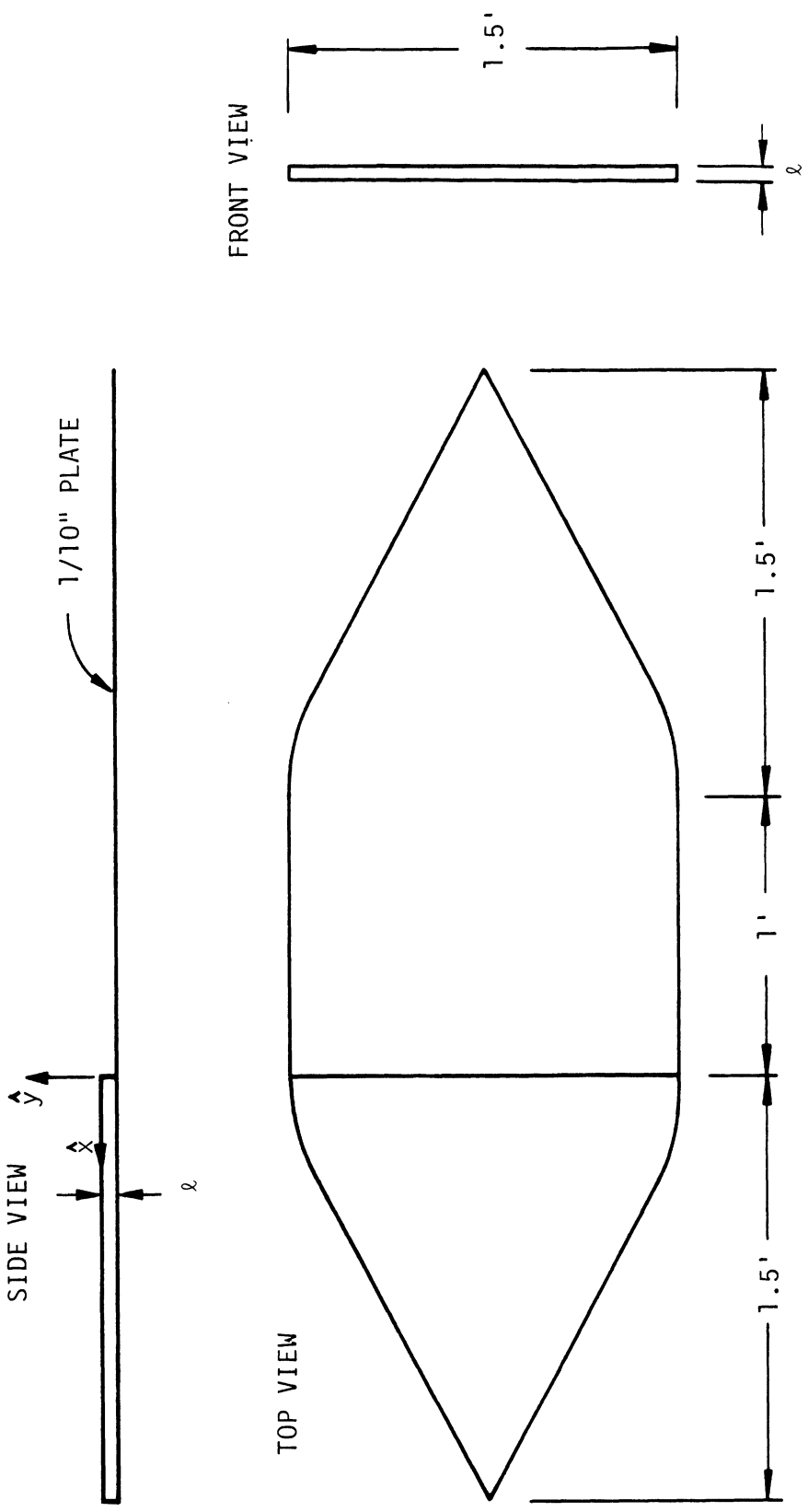

Fig. 8: Measurement Model of a Step Protrusion.

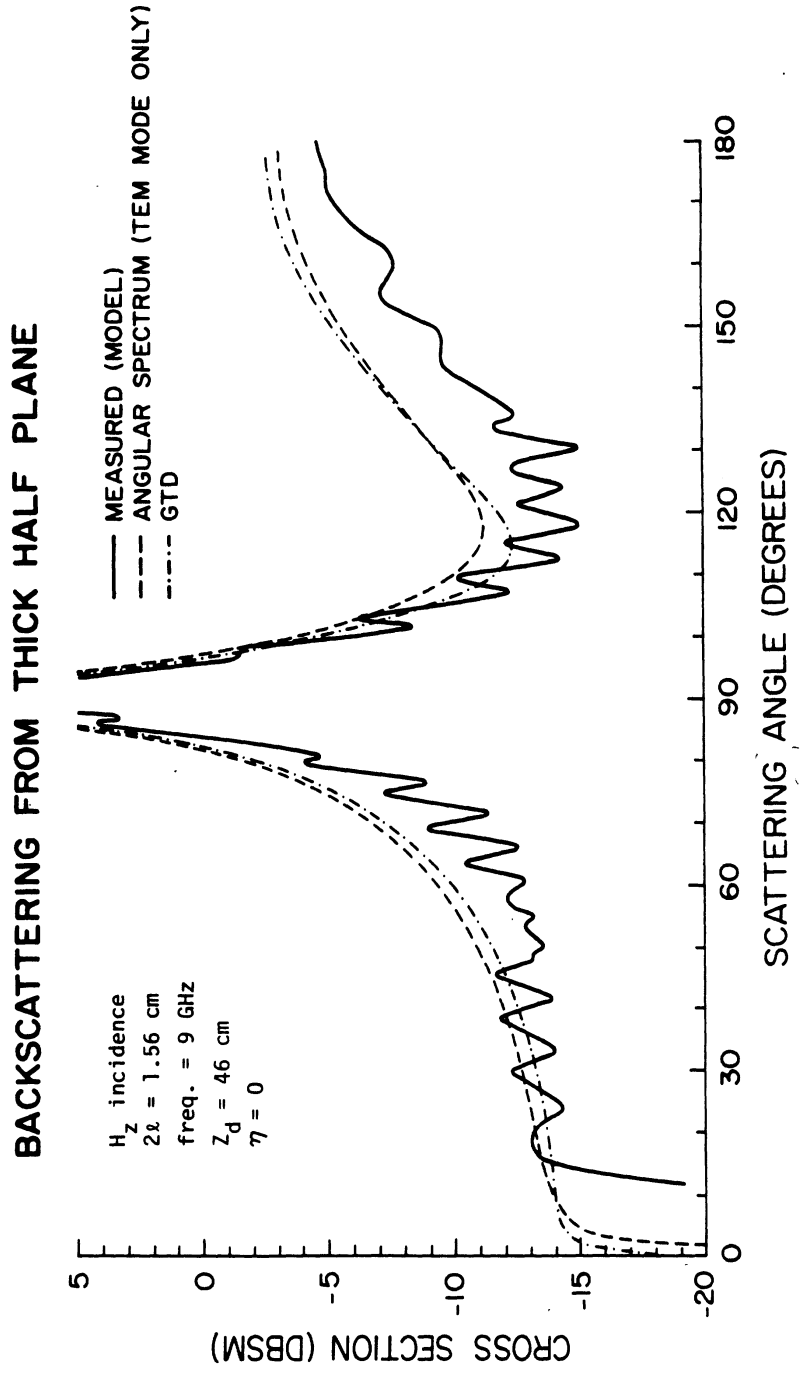

Fig. 9(a): Comparison of measured and calculated backscatter patterns from a perfectly conducting thick edge with 2ℓ = 0.614 inch. (a) H_z incidence.

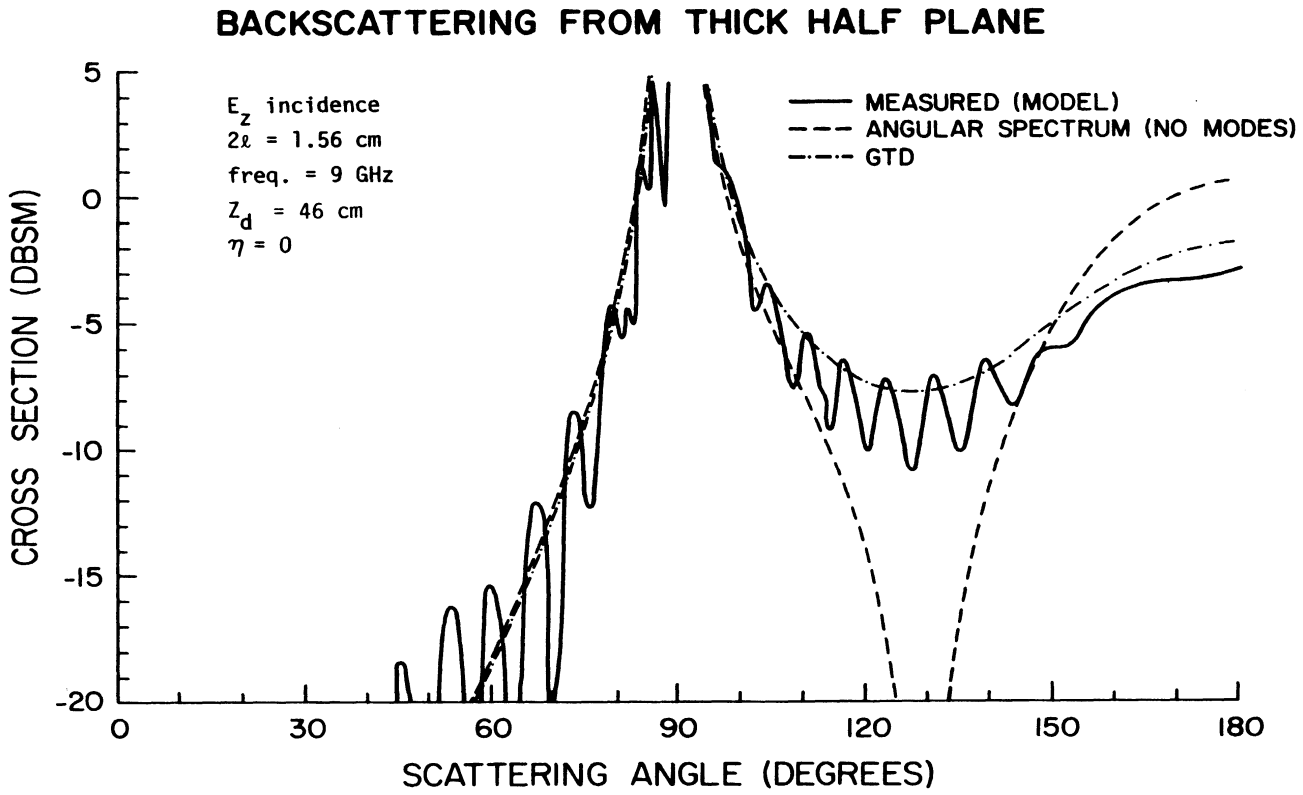

Fig. 9(b): Comparison of measured and calculated backscatter patterns from a perfectly conducting thick edge with 2ℓ = 0.614 inch. (b) E_z incidence.

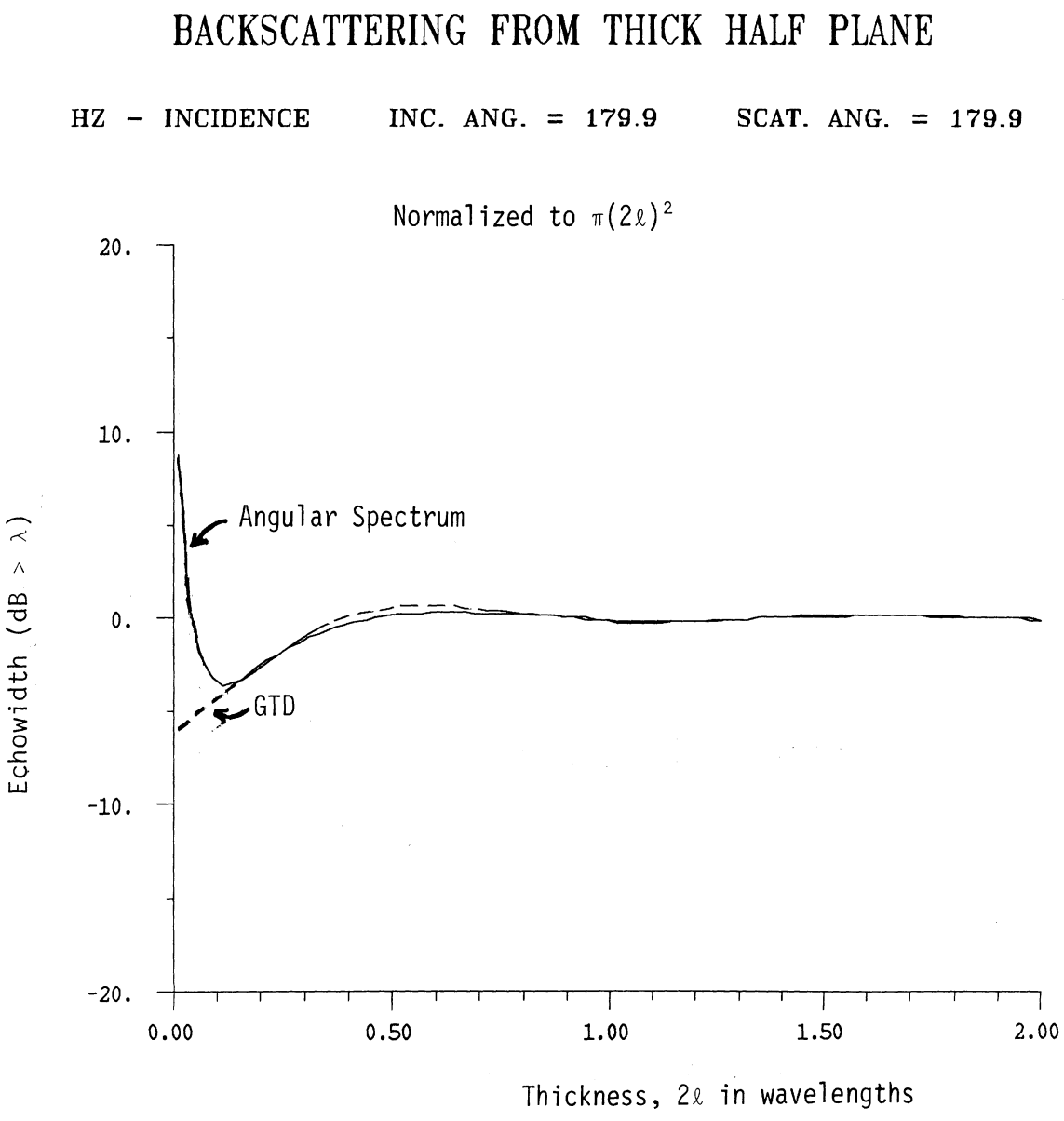

Fig. 10: Echowidth of a thick perfectly conducting edge as a function of its thickness $2\ell/\lambda$.

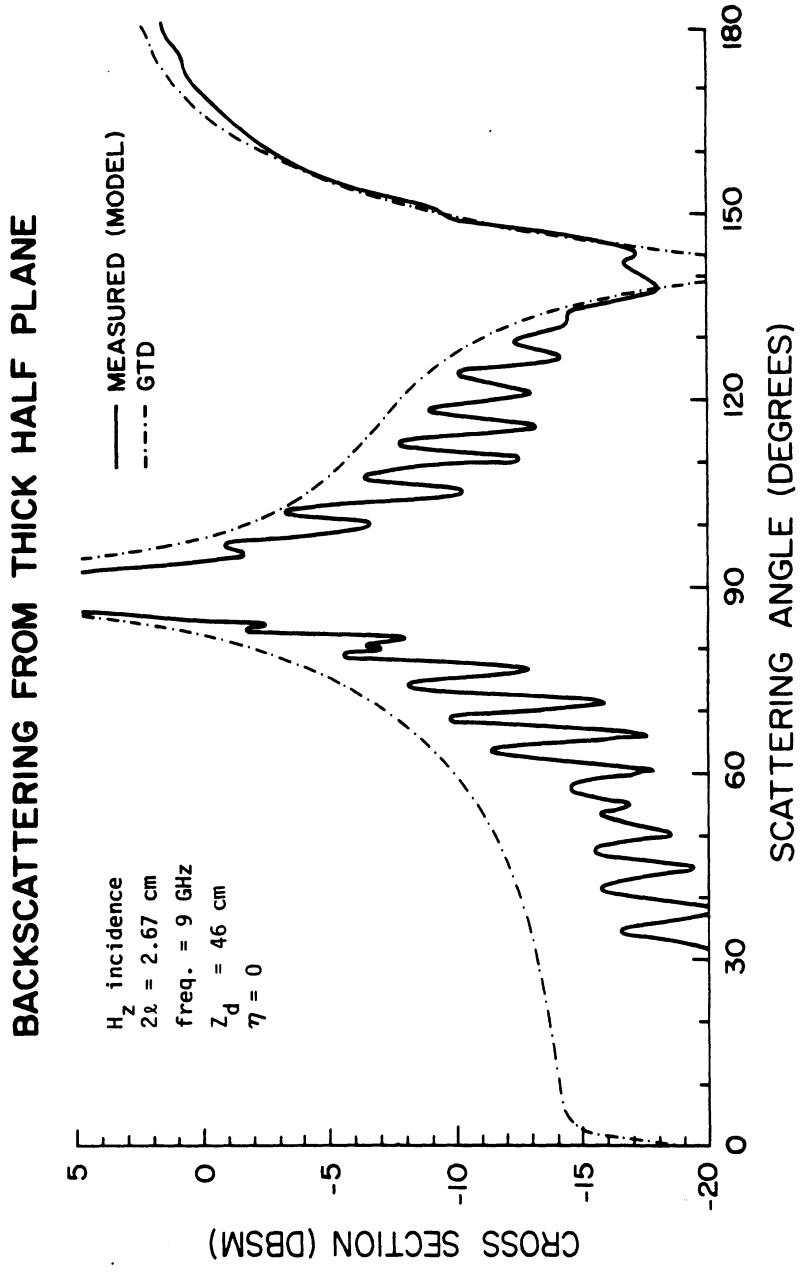

Fig. 11(a): Comparison of measured and calculated backscatter patterns from a perfectly conducting thick edge with 2ℓ = 1 inch. (a) H_z incidence.

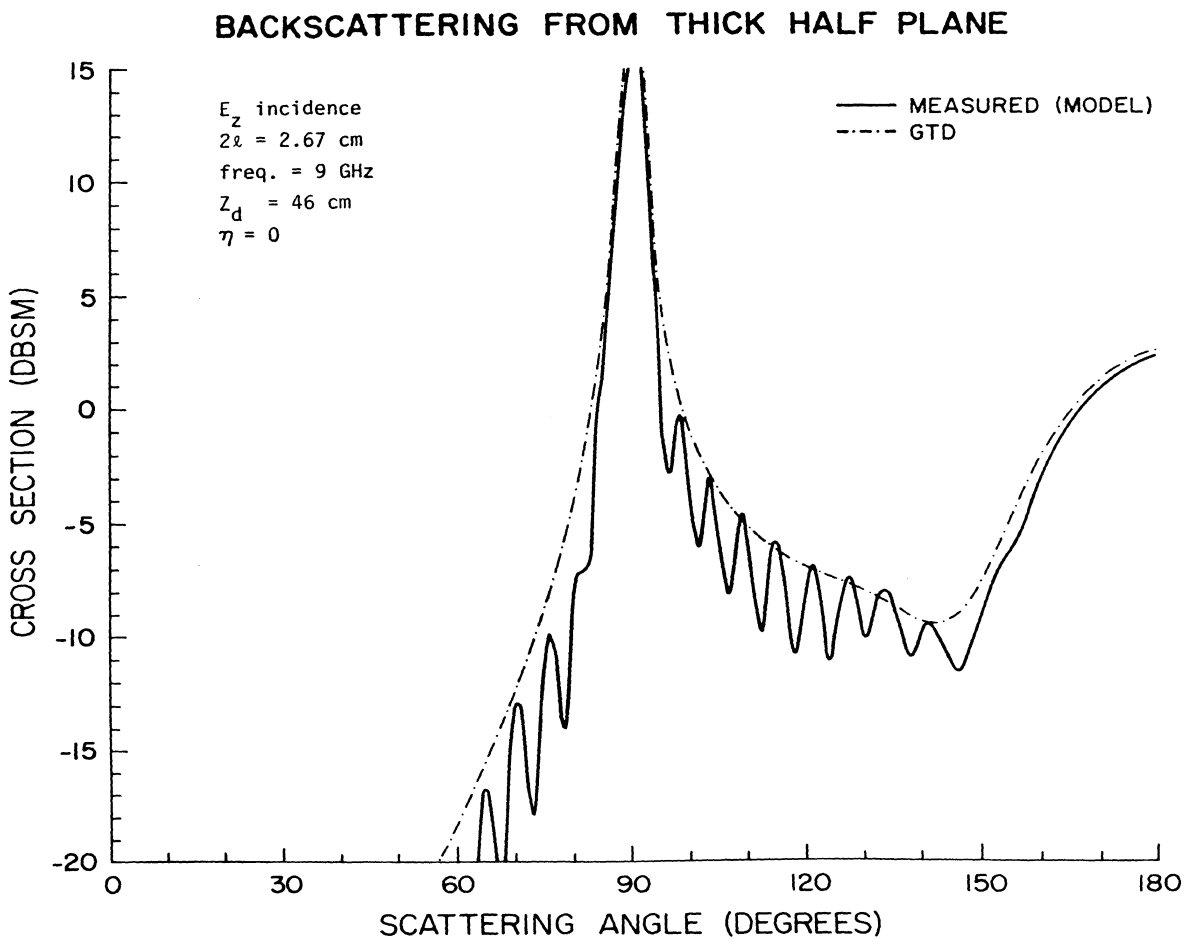

Fig. 11(b): Comparison of measured and calculated backscatter patterns from a perfectly conducting thick edge with 2ℓ = 1 inch. (b) E_z incidence.

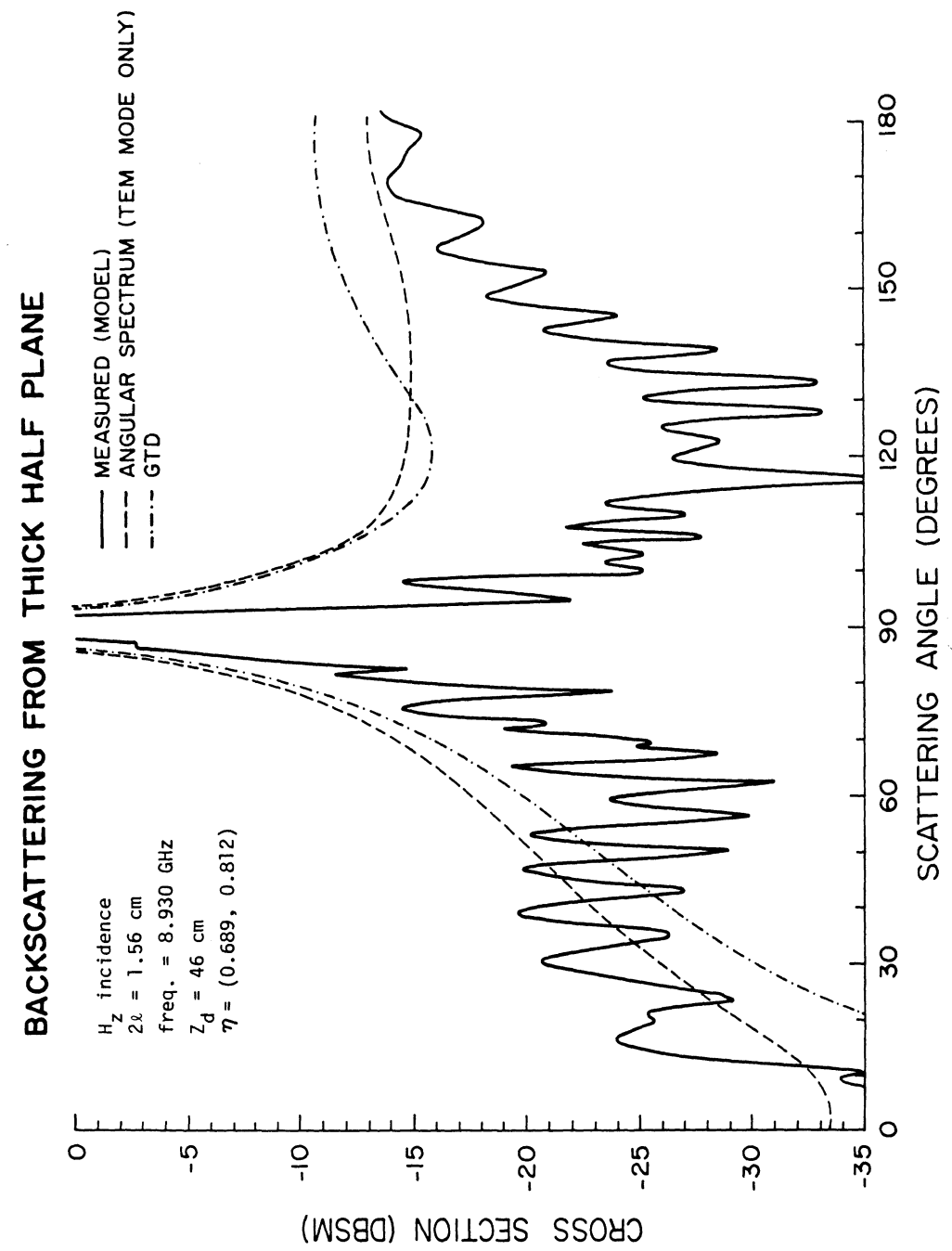

Fig. 12(a): Comparison of measured and calculated patterns from an imperfect edge with η = 0.689+j.812 and thickness 2ℓ = 0.614 inch. (a) H_z incidence.

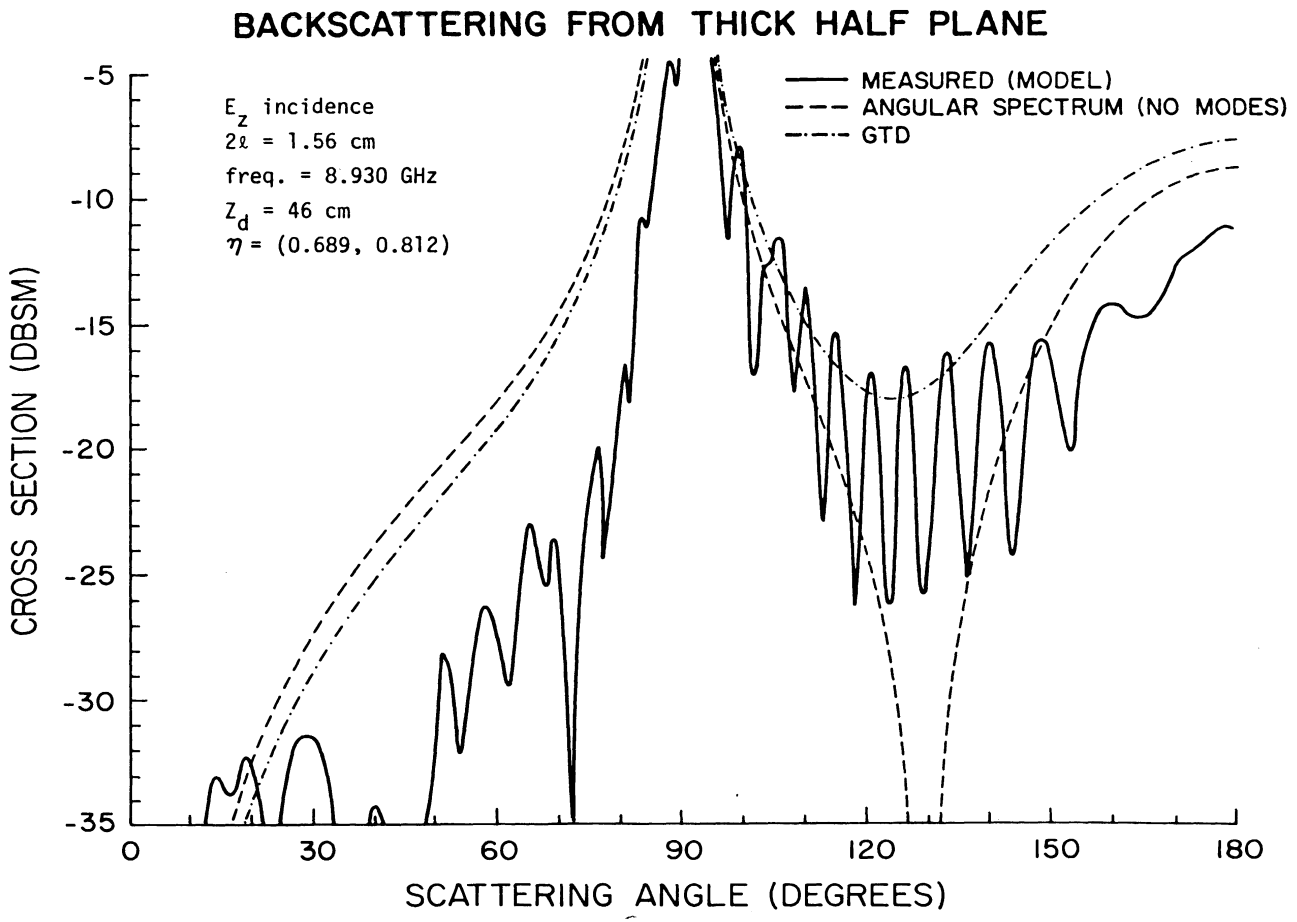

Fig. 12(b): Comparison of measured and calculated patterns from an imperfect edge with η = 0.689+j.812 and thickness 2ℓ = 0.614 inch. (b) E_z incidence.

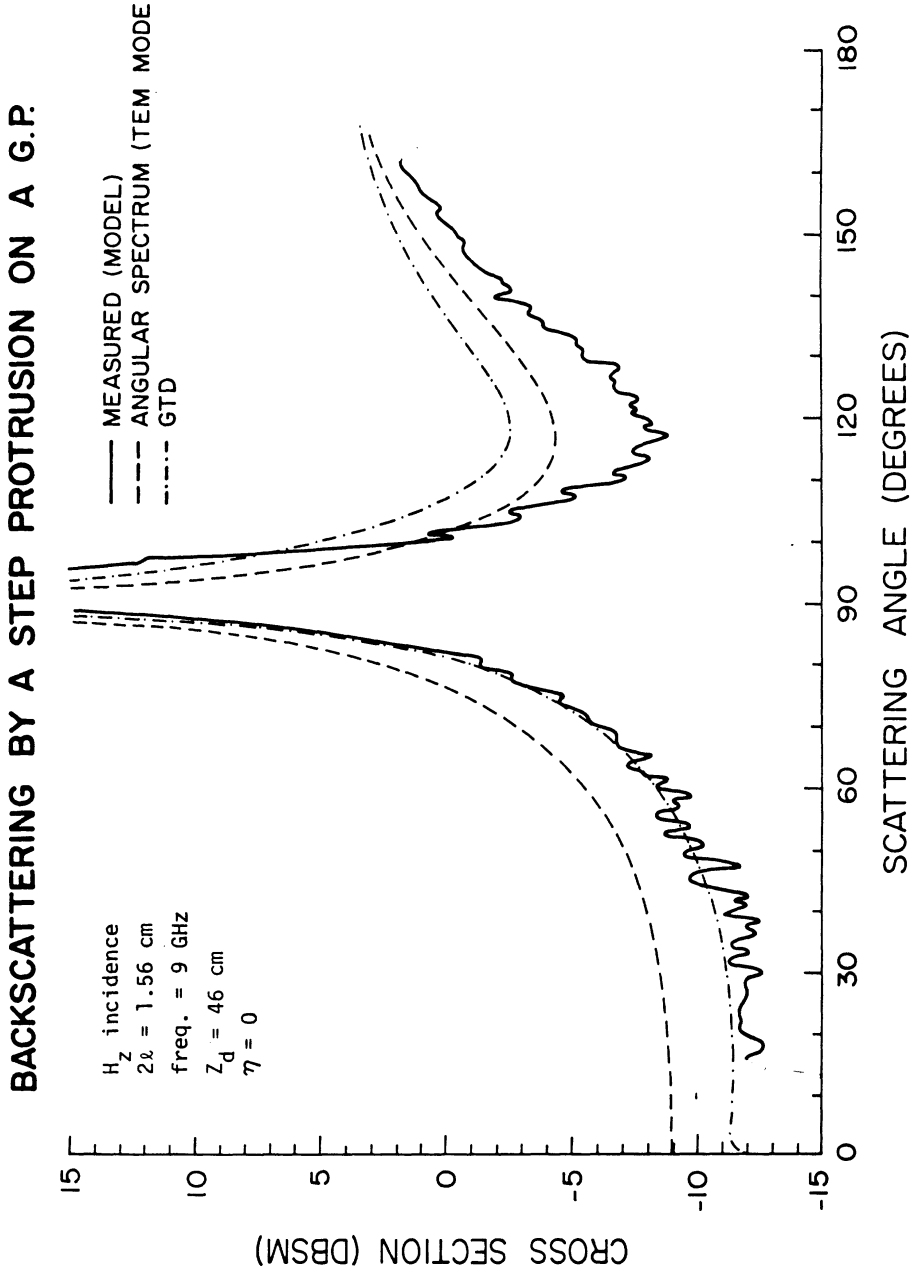

Fig. 13(a): Comparison of measured and calculated patterns for a perfectly conducting step protrusion with ℓ = 0.307 inch. (a) H_z incidence.

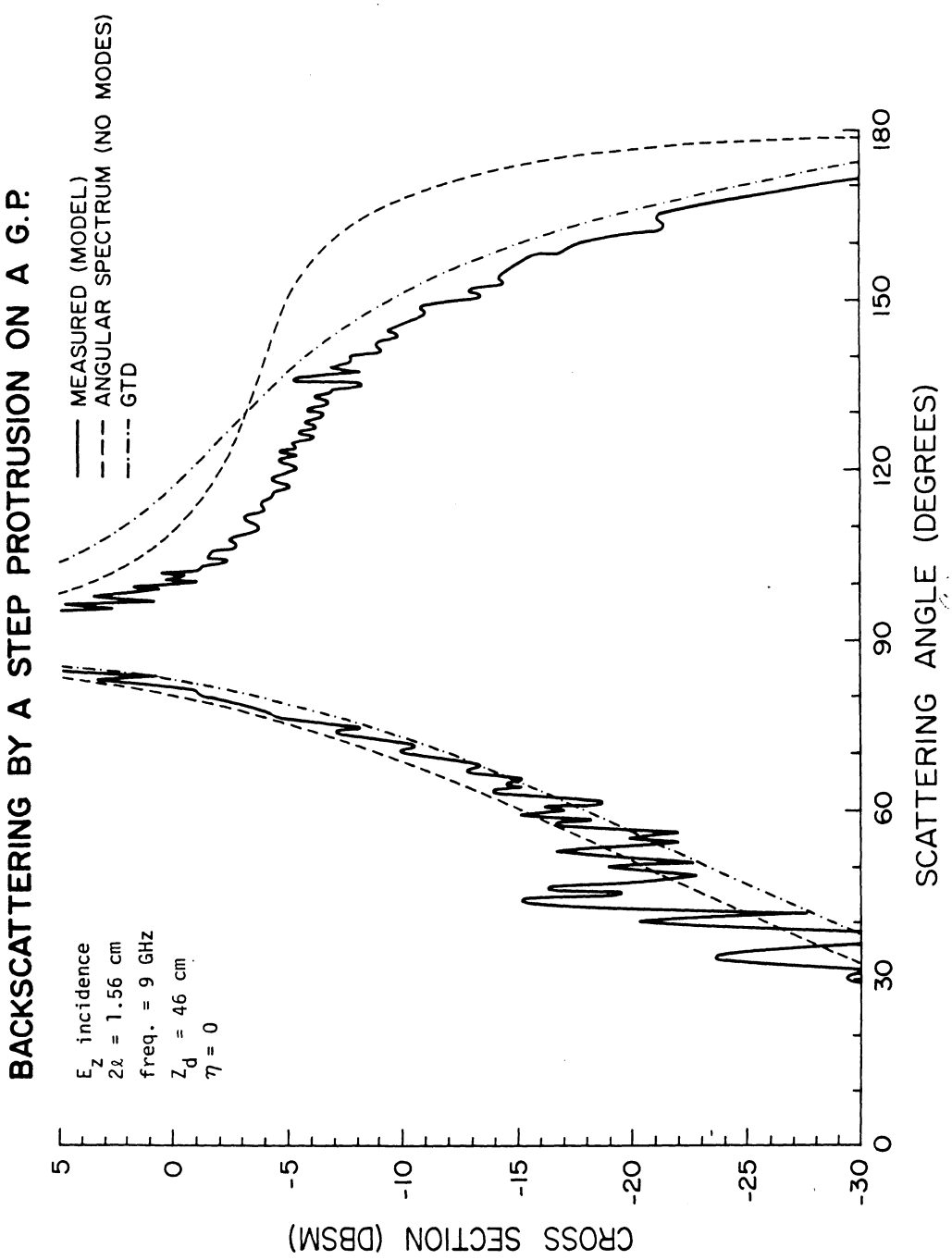

Fig. 13(b): Comparison of measured and calculated patterns for a perfectly conducting step protrusion with ℓ = 0.307 inch. (b) E_z incidence.

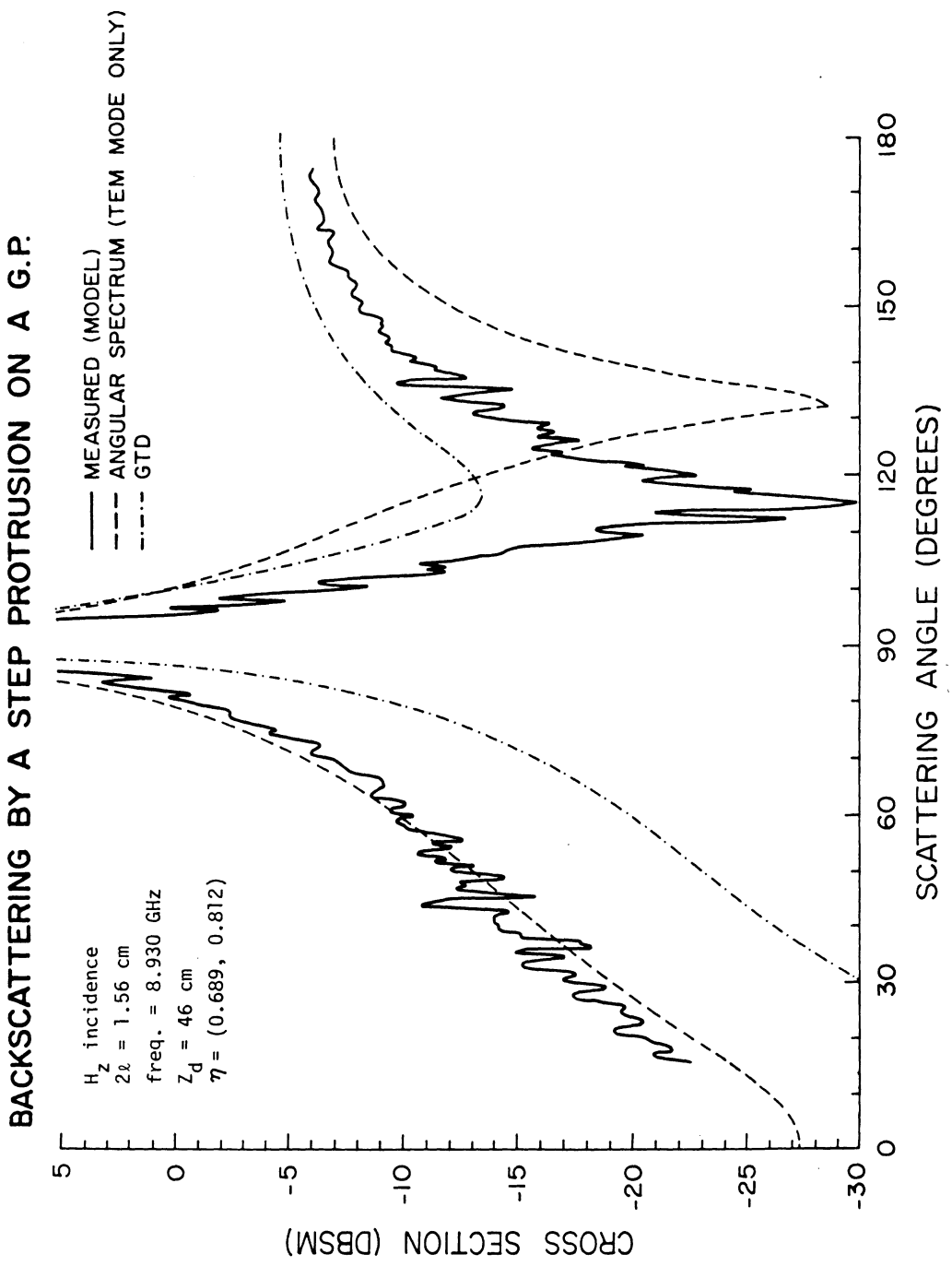

Fig. 14(a): Comparison of measured and calculated patterns from an imperfect step protrusion η = 0.689+j.812 and ℓ = 0.307 inch. (a) H_z incidence.

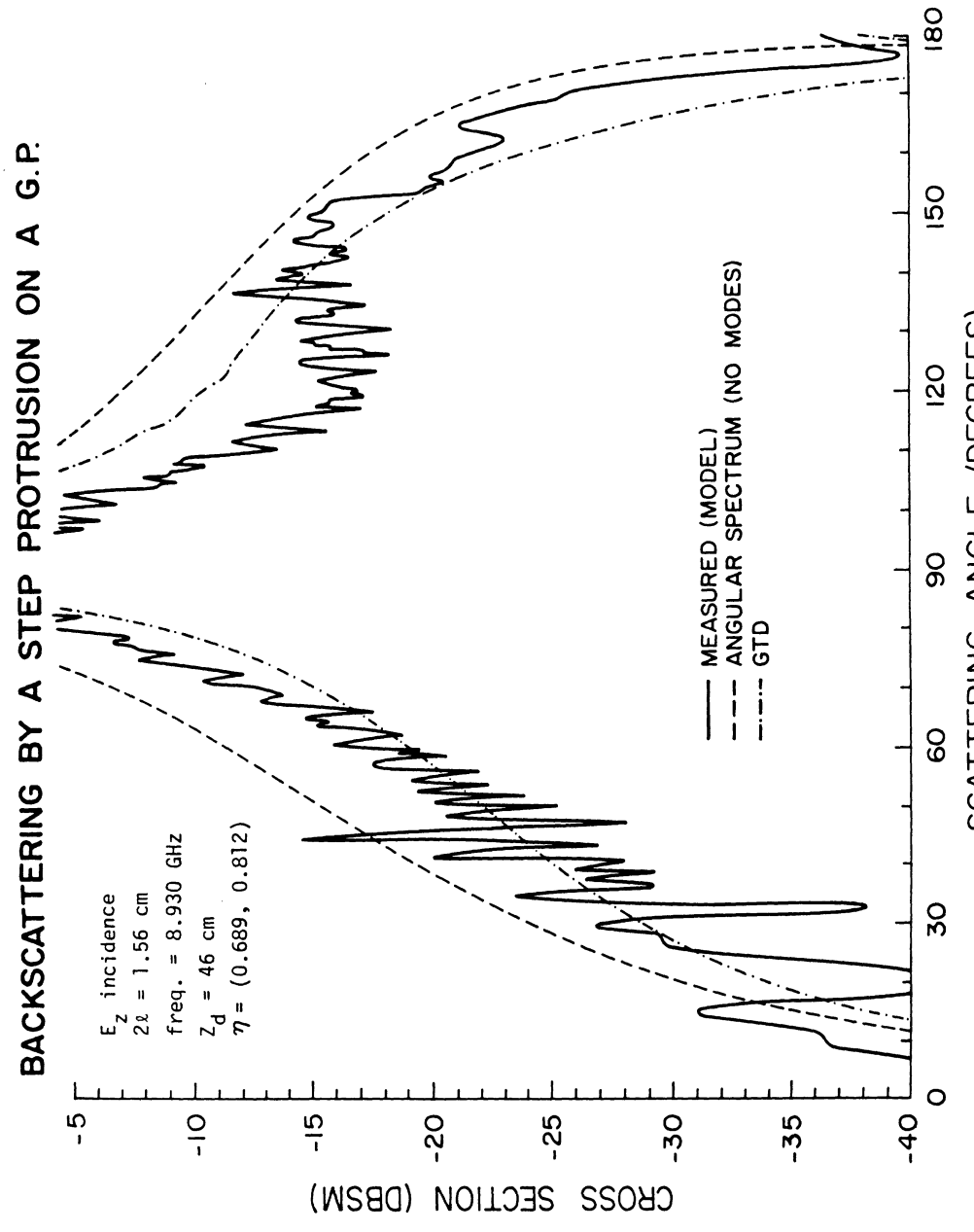

Fig. 14(b): Comparison of measured and calculated patterns from an imperfect step protrusion $\eta = 0.689+j.812$ and $\ell = 0.307$ inch. (b) E_z incidence.

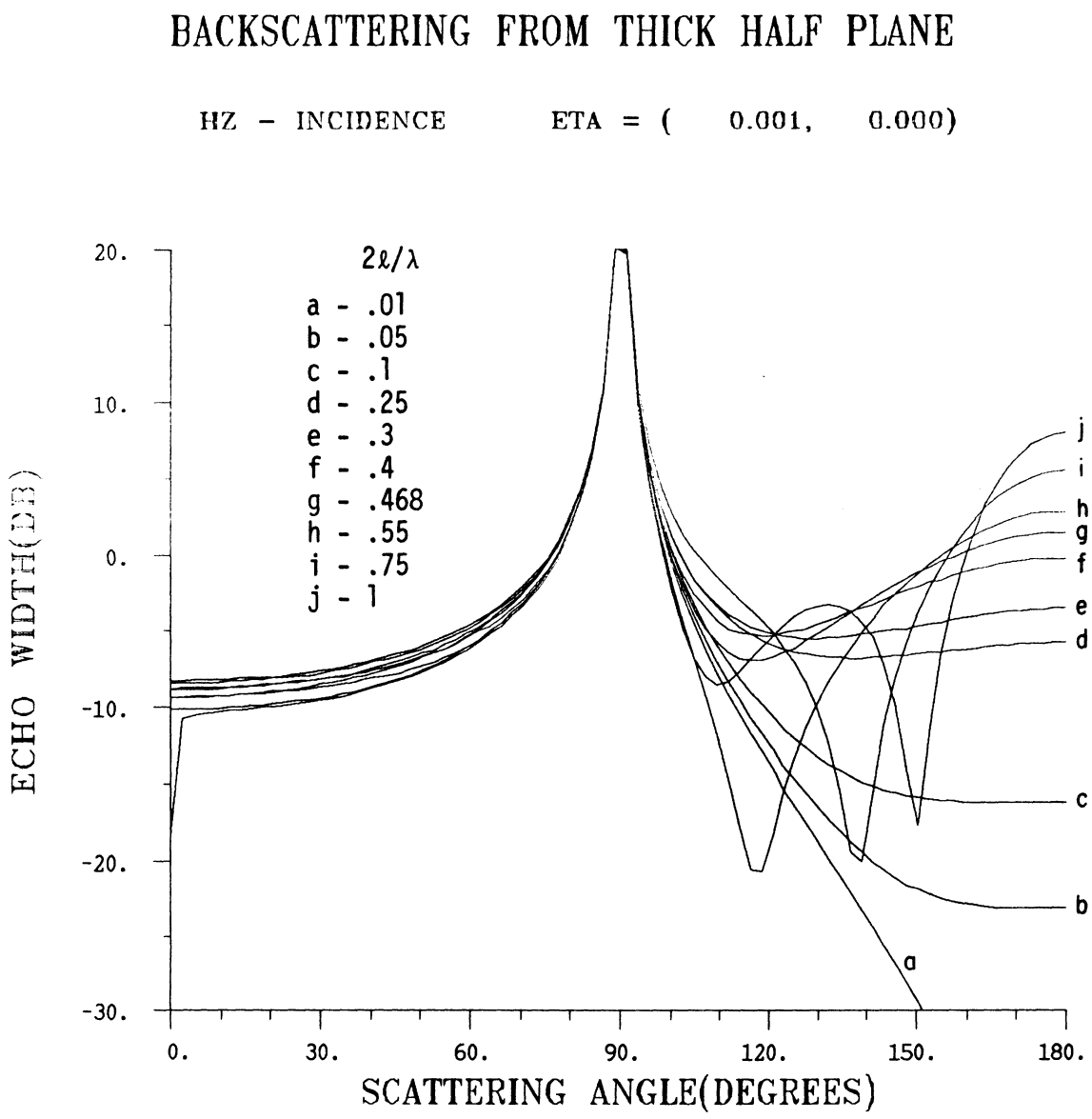

Fig. 15(a): Echowidth of a thick perfectly conducting edge for various values of the edge thickness, 2ℓ. (a) H_z incidence.

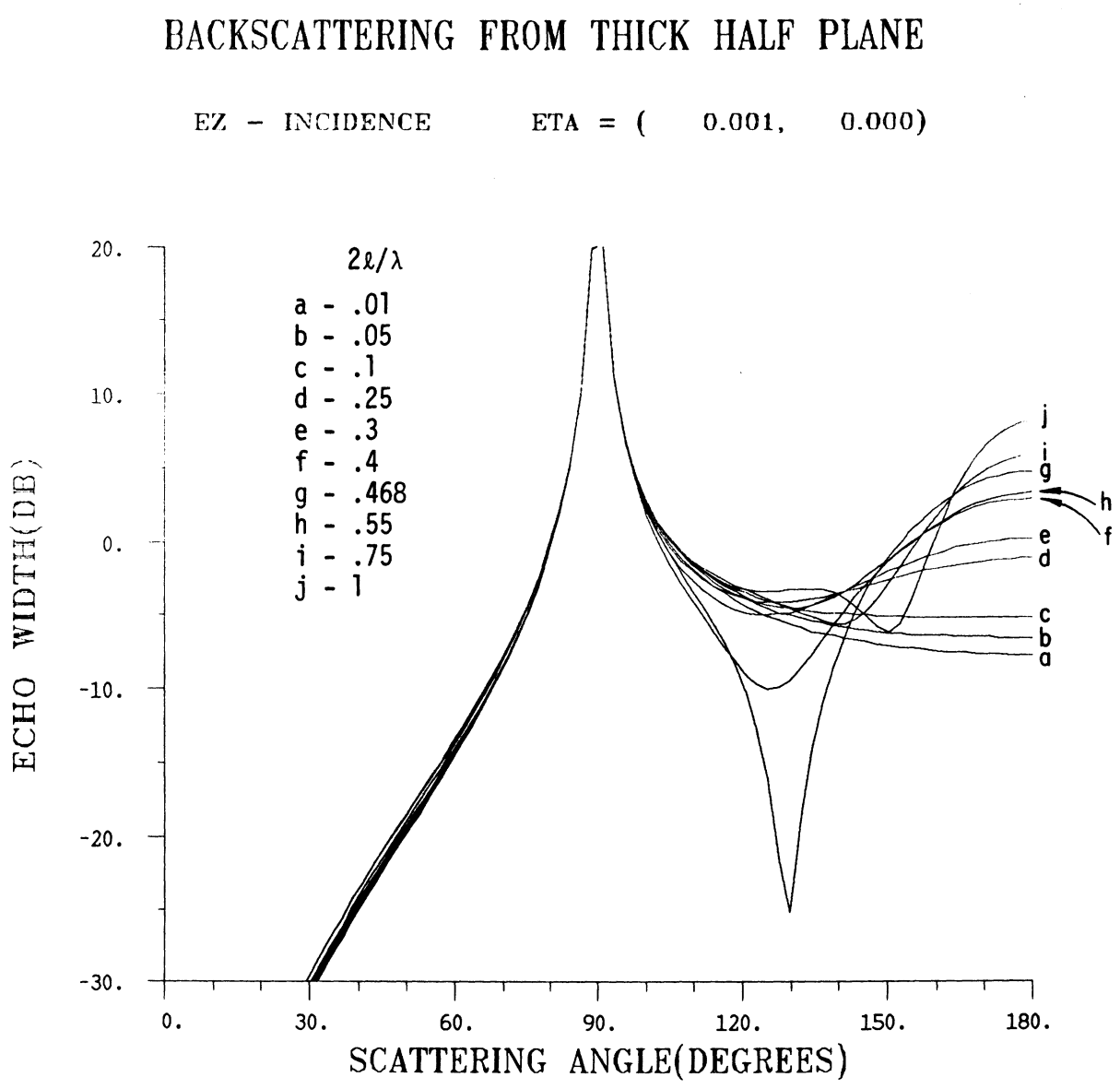

Fig. 15(b): Echowidth of a thick perfectly conducting edge for various values of the edge thickness, 2ℓ. (b) E_z incidence.

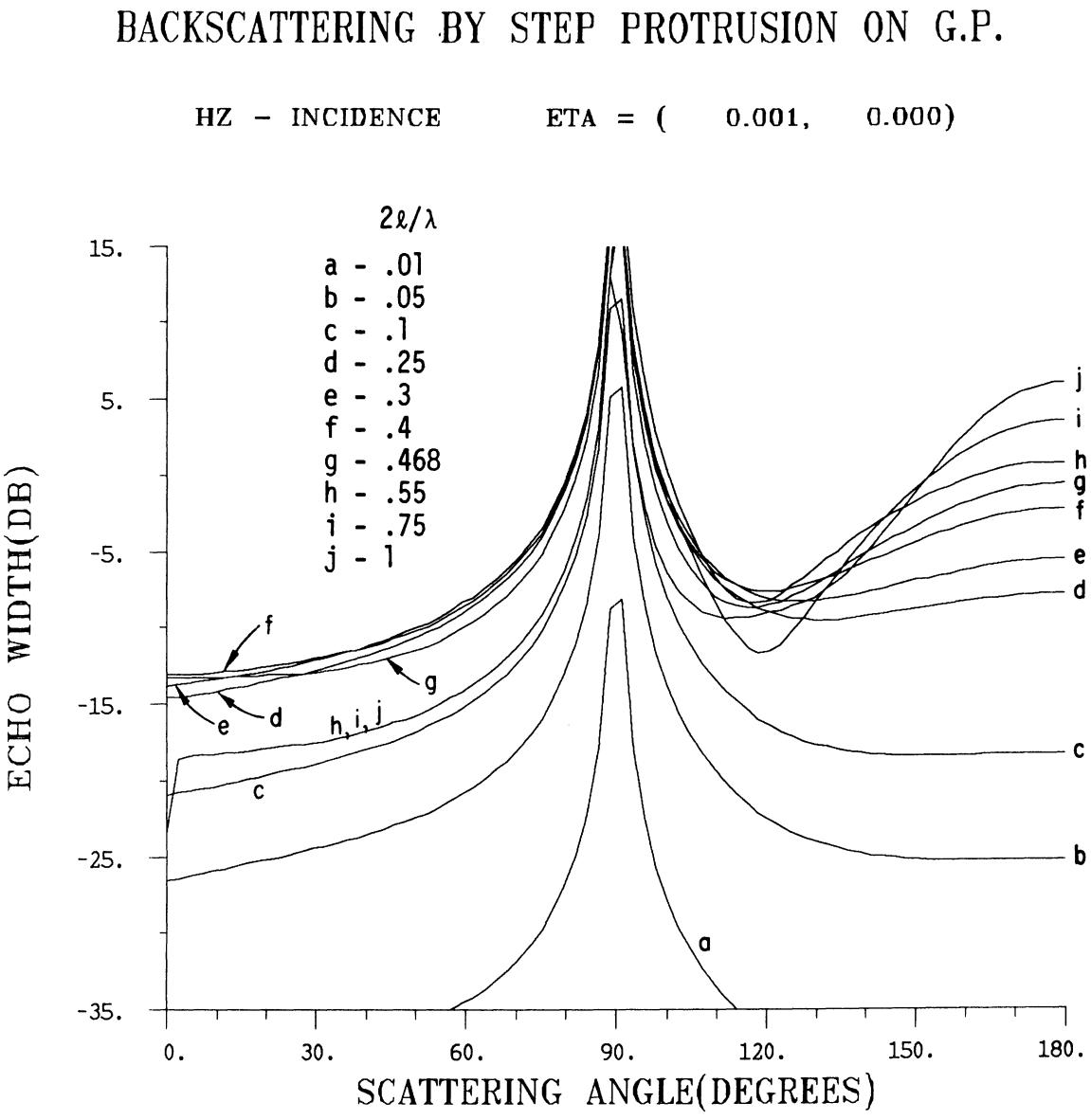

Fig. 16(a): Echowidth of a perfectly conducting step protrusion on a ground plane for various values of the step heighth, ℓ. (a) H_z incidence.

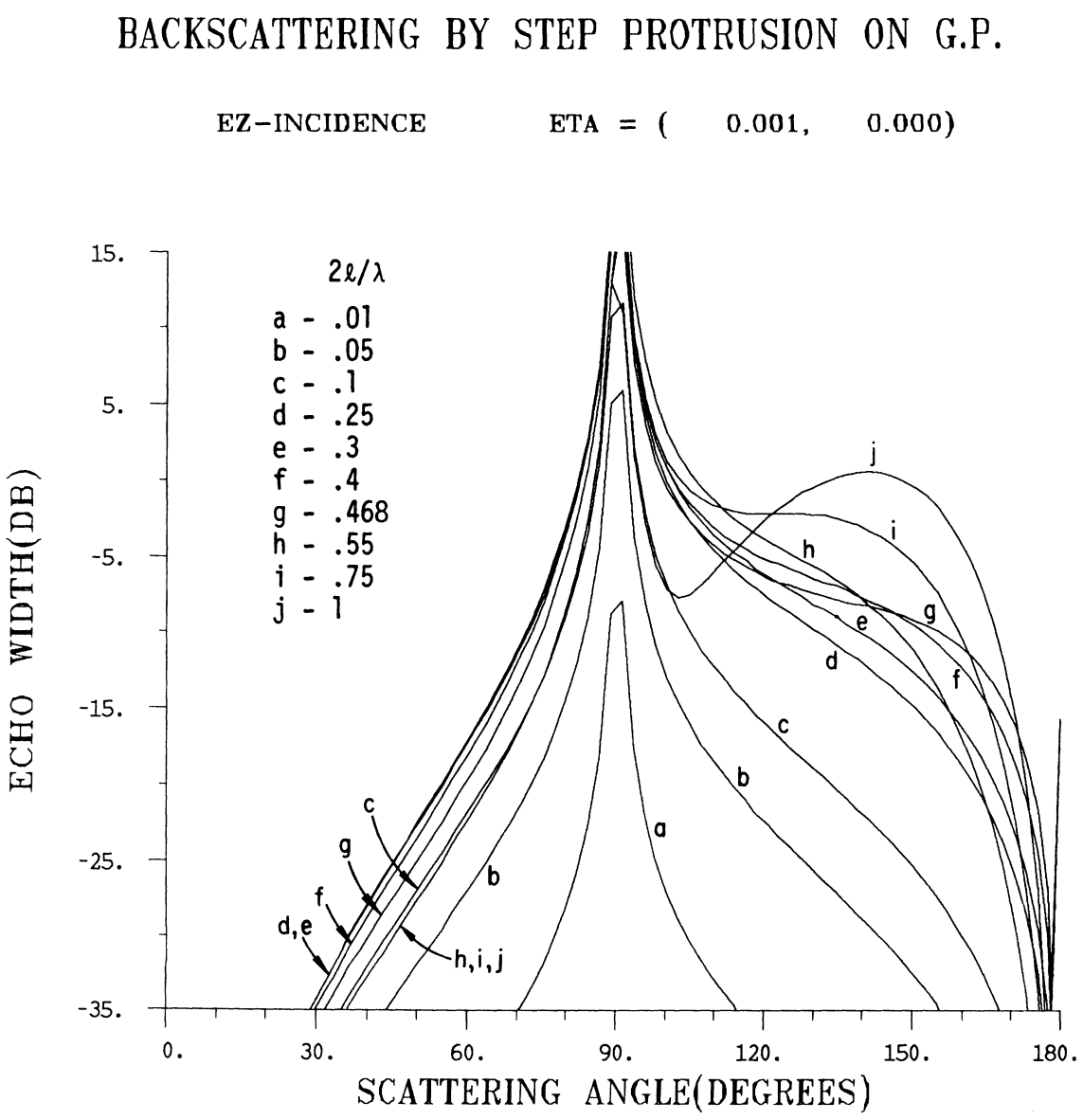

Fig. 16(b): Echowidth of a perfectly conducting step protrusion on a ground plane for various values of the step heighth, ℓ. (b) E_z incidence.

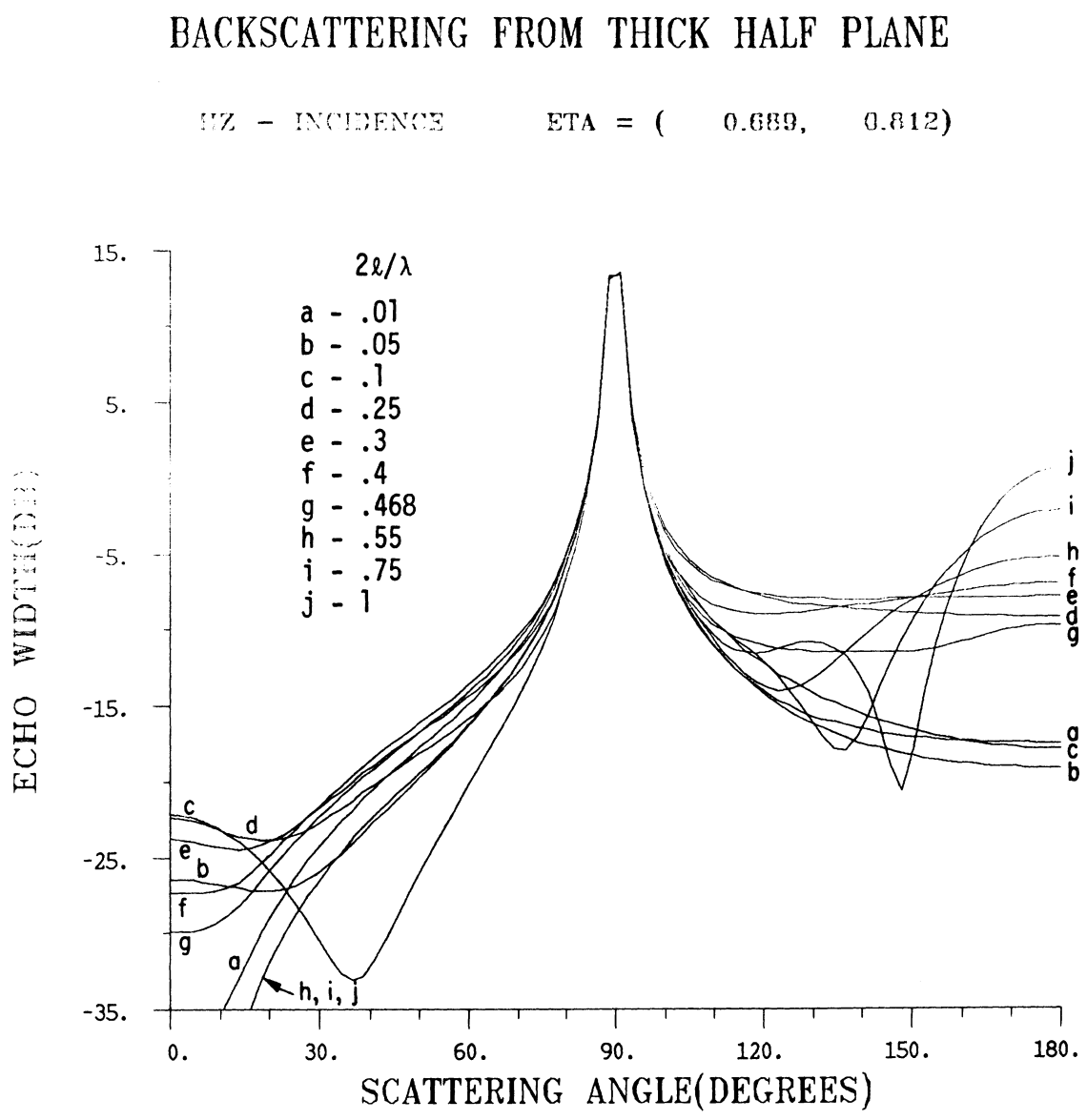

Fig. 17(a): Echowidth of an imperfect edge (η = 0.689+j.812) for various values of the edge thickness, 2ℓ. (a) H_z incidence.

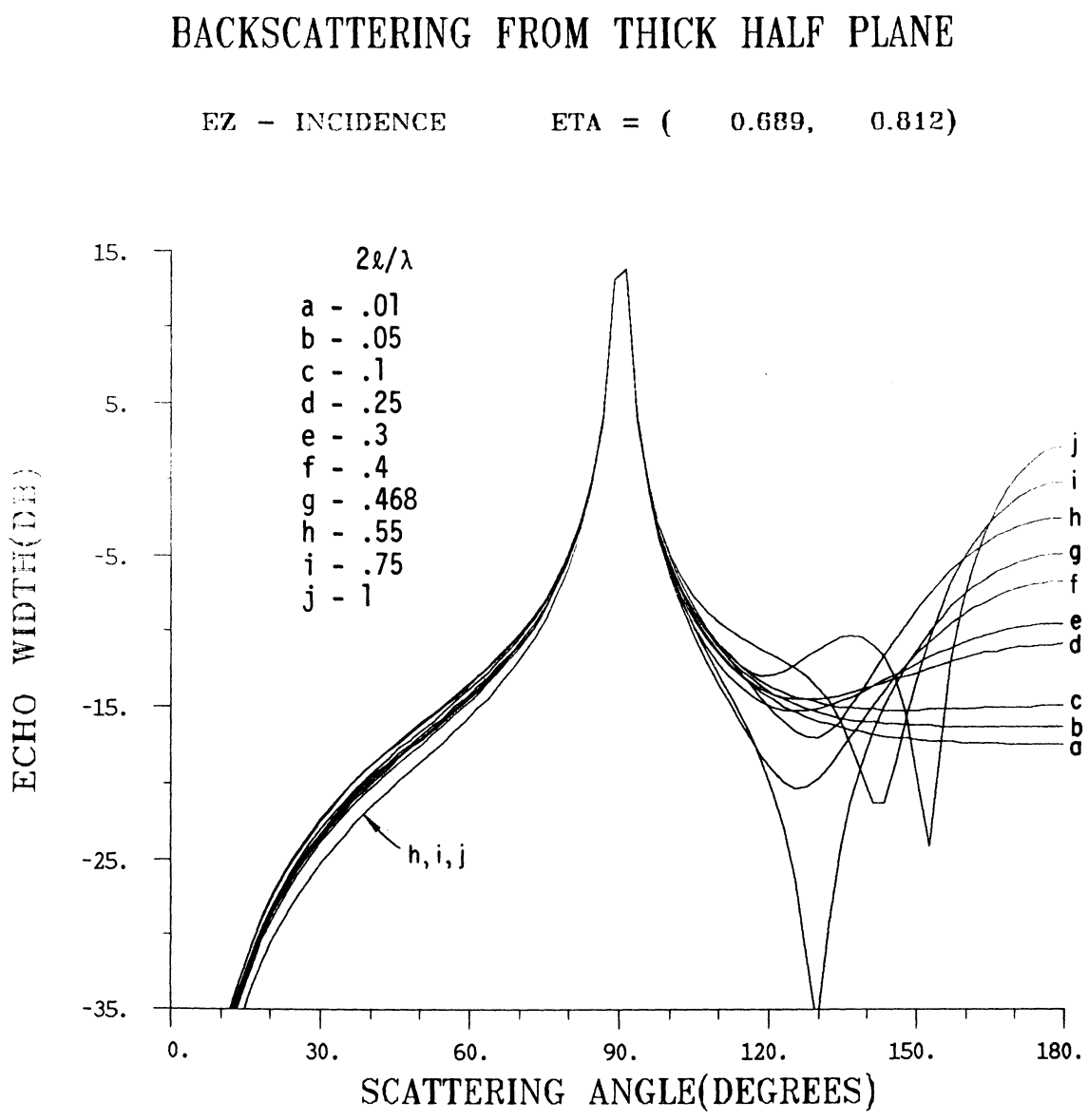

Fig. 17(b): Echowidth of an imperfect edge ($n = 0.689+j.812$) for various values of the edge thickness, 2ℓ. (b) E_z incidence.

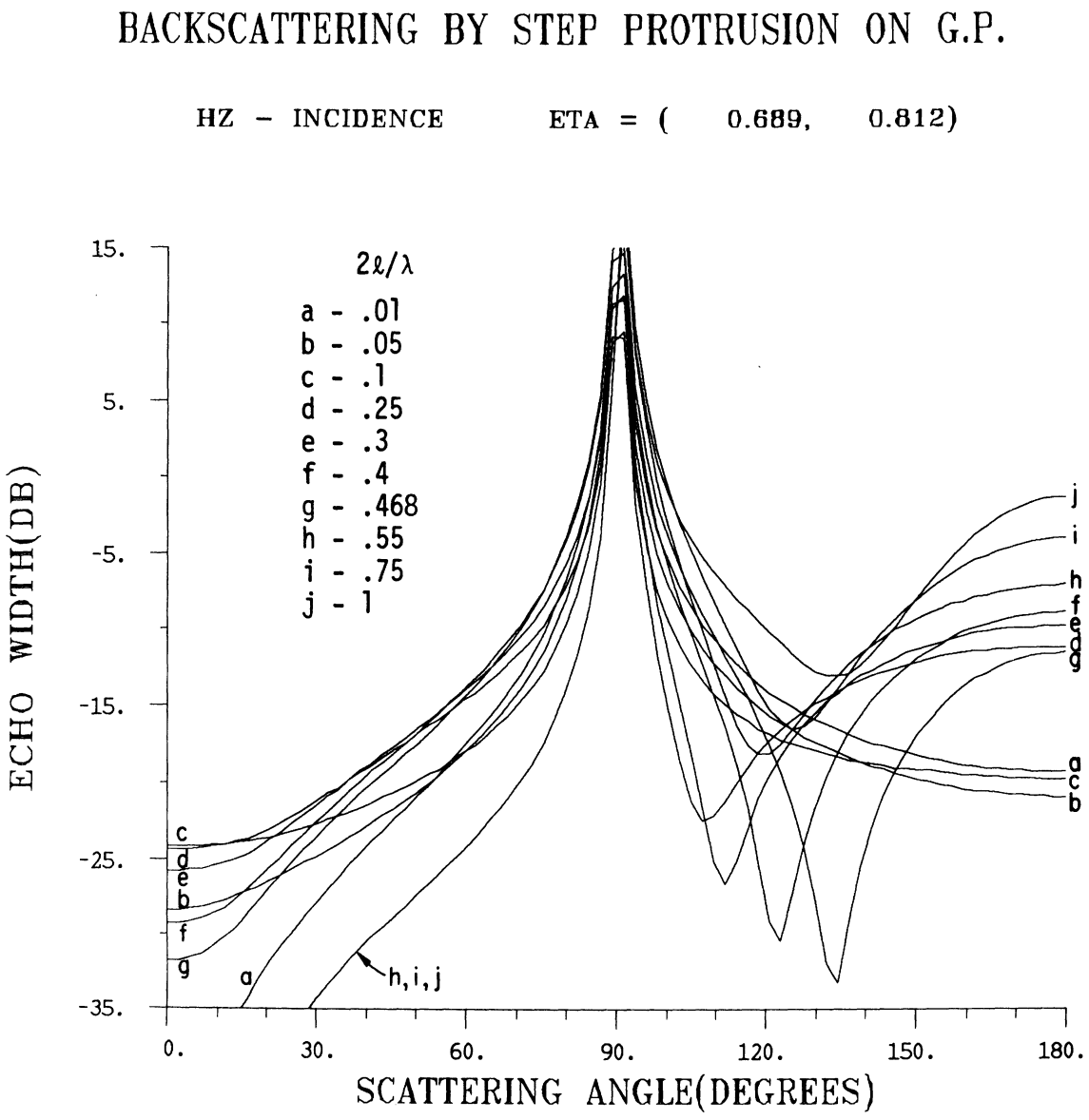

Fig. 18(a): Echowidth of an imperfect step protrusion (η = 0.689+j.812) for various values of the step heighth, ℓ. (a) H_z incidence.

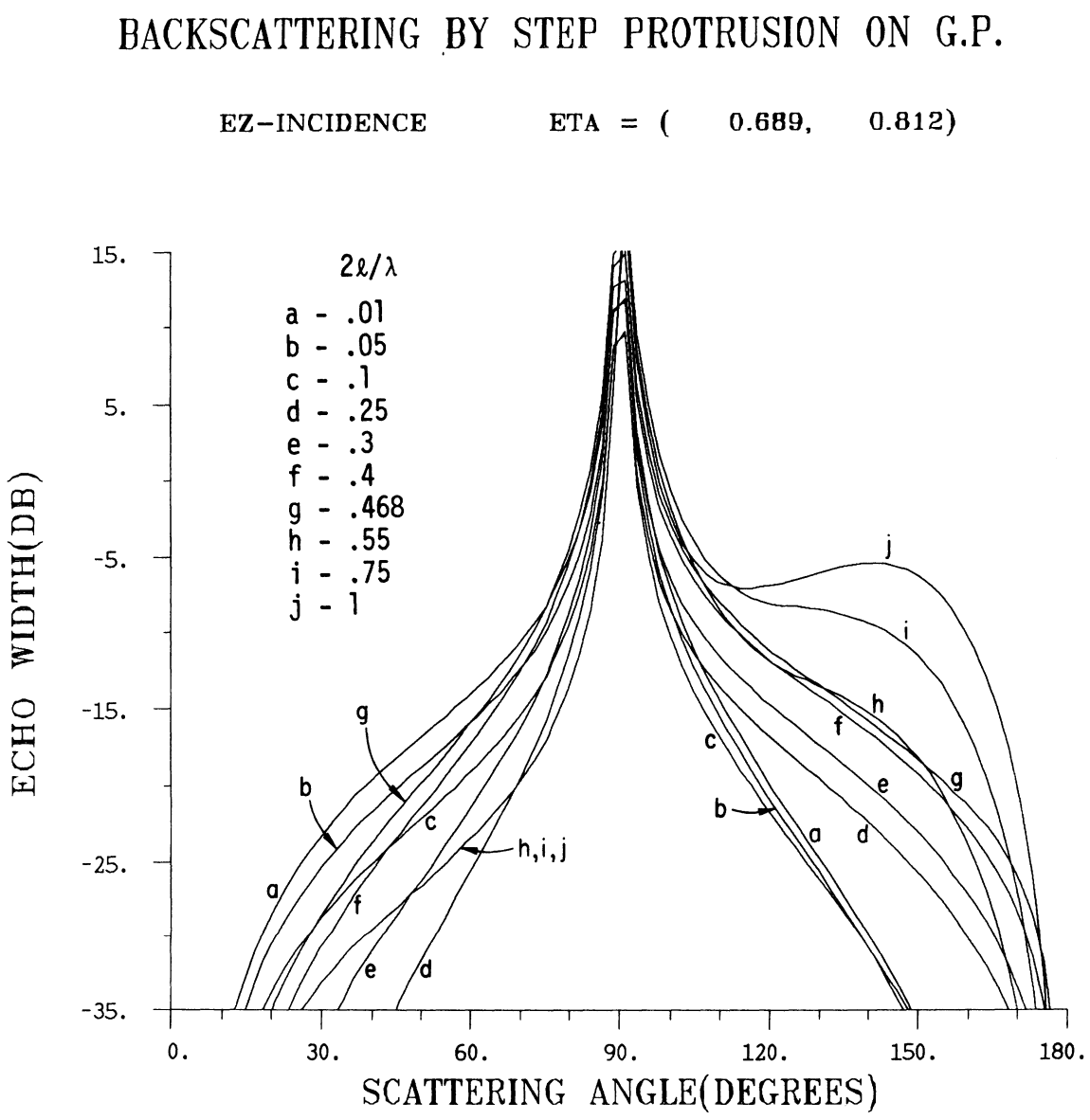

Fig. 18(b): Echowidth of an imperfect step protrusion (η = 0.689+j.812) for various values of the step heighth, ℓ. (b) E_z incidence.